Development of a multi-scale finite element model of the osteoporotic lumbar vertebral body for the investigation of apparent level vertebra mechanics and micro-level trabecular mechanics.

K. McDonald, J. Little, M. Pearcy, C. Adam
Institute of Health and Biomedical Innovation
Queensland University of Technology, Brisbane, Australia

Corresponding author
Associate Professor Clayton Adam
Institute of Health and Biomedical Innovation
Queensland University of Technology
GPO Box 2434, 2 George St
Brisbane Q4001 AUSTRALIA
Phone +61 7 3138 9041
Fax +61 7 3138 8381
Email c.adam@qut.edu.au

Abstract

Osteoporotic spinal fractures are a major concern in ageing Western societies. This study develops a multi-scale finite element (FE) model of the osteoporotic lumbar vertebral body to study the mechanics of vertebral compression fracture at both the apparent (whole vertebral body) and micro-structural (internal trabecular bone core) levels. Model predictions were verified against experimental data, and found to provide a reasonably good representation of the mechanics of the osteoporotic vertebral body. This novel modelling methodology will allow detailed investigation of how trabecular bone loss in osteoporosis affects vertebral stiffness and strength in the lumbar spine.

Keywords

Finite Element, osteoporosis, vertebral mechanics, trabecular mechanics, multi-scale model, vertebral compression fracture.

Introduction

Osteoporosis is a disease characterized by low bone mass and micro-architectural deterioration of bone tissue, with a consequent increase in bone fragility and susceptibility to fracture[1]. Osteoporosis affects over 200 million people worldwide[2], with an estimated 1.5 million fractures annually in the United States alone[3], and with attendant costs exceeding $10 billion per annum[4]. Although osteoporosis affects the entire skeleton, many osteoporotic fractures occur in the vertebrae of the spine[5]. In particular, spinal fractures are associated with the highest risk of death after an osteoporotic fracture. The mortality rate in the first year after a vertebral fracture is 28%, rising to 72% after five years[6]. Osteoporotic vertebral compression fractures (VCFs) affect one in four women aged 50 and over, the prevalence increasing to become almost universal by the eighth decade. VCFs are associated with pain, reduced mobility, and increased morbidity[7,8].

The vertebra (Figure 1) is comprised of an anterior vertebral body, and posterior elements. The vertebral body is the primary compressive load bearing structure in the spine, and adjacent vertebral bodies are connected by soft intervertebral discs (not shown in Figure 1) which impart flexibility to the spine. The vertebral body itself comprises a lattice-like porous internal trabecular bone core, surrounded by a thin shell (cortex) of dense cortical bone.

Previous studies have shown that the trabecular bone core carries a substantial proportion of the compressive load in the vertebral body[9,10]. From an engineering perspective, trabecular bone is a porous, open cell, living structural material. Trabecular bone is highly metabolically active, and is therefore most susceptible to the bone loss which occurs during osteoporosis. The loss of trabecular bone density and strength

during osteoporosis can lead to collapse of the entire anterior vertebral body, known as a vertebral compression fracture.

The loss of trabecular density occurs through a series of changes to the trabecular micro-structure. Healthy trabecular bone is thick and plate-like; however, with the progression of age and osteoporosis, the trabecular microstructure is thinned, plates of bone are perforated, and the bone transforms into a strut-like lattice[11]. Because bone remodels in response to the loads it encounters, the strut-like structure becomes highly orientated in the direction of loading. This produces weight bearing longitudinal struts (approximately vertical columns aligned normal to the dominant compressive loading direction), connected by thin transverse struts (see Figure 2)[12]. With ongoing bone loss, the spacing between the struts is increased, the strut diameters decrease, and some of the transverse connections are broken, making the new poorly connected structure particularly susceptible to buckling failure[13].

Due to the complex anatomy of the vertebral body and limited availability of cadaveric specimens, Finite Element (FE) models have been widely used to investigate vertebral body mechanics. However, with the exception of large scale voxel-based models developed by one group (see for example Adams *et al*[14]), all FE models of the vertebral body to date have been macro-scale models, simplifying the complex trabecular bone microstructure as a continuum with either isotropic linear elastic[15,16,17], or elasto-plastic[18,19] constitutive properties. At the micro-scale, FE models of small volumes of trabecular bone have been developed to investigate the effect of changes in micro-

structure on apparent level[A] trabecular bone properties[20,21], but these models have not been coupled to the macro-scale compressive failure behaviour of the whole osteoporotic vertebral body. While prior modelling approaches at both scales have provided insights into the mechanisms of vertebral compression fractures with progressive bone loss in osteoporosis, they have not allowed parametric investigation of how micro-scale strut buckling and deformation processes in trabecular bone lead to overall vertebral body collapse. The mechanics of the osteoporotic vertebral body are affected by the micro-structure of the trabecular core, and the mechanics of the trabecular micro-structure are affected by how it is loaded within the vertebral body. Accordingly, the aim of this study was to develop a multi-scale FE model of the osteoporotic lumbar vertebral body to allow simultaneous investigation of apparent level vertebral mechanics and microstructural level trabecular bone mechanics.

Methods

A lattice model was chosen to represent the trabecular micro-structure, as the rod-like nature of osteoporotic trabecular bone lends itself to be described by a three dimensional array of longitudinal and transverse struts. A number of other approaches, such as voxel-based models[22,23], skeletonised graphs[24], and Voronoi diagrams[25,26], have previously been used. However, a lattice provides a high degree of control over the micro-structure with minimal computational expense, allowing large structures to be modelled. The model development process was as follows; firstly, an individual trabeculae (single longitudinal strut) FE model was developed and verified to ensure that it correctly captured compressive buckling behaviour across a range of slenderness

[A] The term 'apparent level' is used herein to refer to the trabecular bone mechanical properties at the macro-level, i.e. without any reference to the trabecular microstructure. Apparent level stress and strain is defined accordingly based on the overall specimen dimensions and deformation. 'Tissue level' mechanical properties refers to the constituent material at the micro-level, i.e. the bone tissue itself.

ratios representative of those found in osteoporotic trabecular bone. Secondly, the single strut model was then used as the building block for modelling larger trabecular lattice structures, and computed results for this trabecular lattice model were verified against experimental data for cylindrical core specimens of human trabecular bone. Finally, an entire vertebral body was modelled by adding an external vertebral cortex (meshed with shell elements) surrounding the internal trabecular core lattice, with model geometry based on previously described anatomical equations for the human L3 lumbar vertebral body.

Single trabecular strut model

The long, slender struts in osteoporotic trabecular bone are prone to buckling failure under the predominantly compressive loads to which they are subjected. It has been suggested that the mode of failure for trabecular bone varies between plastic collapse (material yield), and elastic buckling (loss of stability of the struts) with aging[13]. Long, thin trabeculae have a high slenderness ratio and are more likely to fail due to elastic buckling, whereas shorter, thicker trabeculae with low slenderness ratio are prone to inelastic buckling or plastic collapse. The mode of failure therefore varies with the degree of osteoporosis of the trabecular microstructure, and it is important for an FE model to accurately represent the buckling response for different trabecular slenderness ratios.

Modelling buckling mechanisms

To capture the failure of longitudinal struts, a single trabecular strut model was produced with an isotropic linear elastic, perfectly plastic von Mises material definition. The von Mises yield surface is defined in Equation [1] below, where σ_1, σ_2, σ_3 are the

maximum, intermediate, and minimum principal stresses respectively, and σ_y is the yield stress.

$$(\sigma_1 - \sigma_2)^2 + (\sigma_2 - \sigma_3)^2 + (\sigma_3 - \sigma_1)^2 = 2\sigma_y{}^2 \qquad \text{Equation [1]}$$

Due to the lack of experimental data for compressive buckling of single trabecular struts, it was not possible to verify the model predictions against trabecular bone buckling data. Therefore, the single strut model predictions were compared with a previous study which reported experimental buckling data for stainless steel columns over a wide range of slenderness ratios[27]. In this study, Rahman *et al.* report compressive failure forces for SUS304 columns of slenderness ratios from 14 to 184, capturing the complete range of column failure mechanisms, including plastic collapse, inelastic buckling failure, and elastic buckling failure[27]. The longitudinal strut FE model geometry was matched to those tested experimentally by Rahman *et al*, and material properties (E=193GPa, ν= 0.27, σ_y=780MPa) were based on compression and tensile material tests performed by Rahman *et al* on their experimental material[27]. Based on the results of a preliminary mesh sensitivity analysis the columns were modelled using two quadratic beam elements, and an initial imperfection was included at the centre of the column (0.001mm offset) to allow buckling initiation. The boundary conditions applied to the model replicated the clamped boundary conditions and axial compressive displacement applied experimentally. The models were solved using ABAQUS/Standard, Version 6.7 (Simulia, RI, USA) with a quasi-static solution procedure, and the nonlinear geometry function enabled for finite deformations. The predicted failure force for each model was compared to the experimentally measured

failure force for the corresponding slenderness ratio column. As the experimental data consisted of tests on three samples for each column, the experimental results for each column were averaged to provide one mean value for comparison.

Trabecular core lattice model

Lattice representation of the trabecular microstructure

Following development and validation of the single trabecular strut model, the model was extended to generate a lattice network representing a three dimensional trabecular bone structure. The perturbed tetragonal lattice was generated using custom Matlab code (version 7.1, Mathworks, Natick, MA, USA) which specified the vertices of the lattice, and then generated finite elements between the vertex points. The trabecular bone microstructure was based on data reported by Mosekilde[28], who characterised trabecular bone micro-structure for three age groups (age < 50yr, age 50-75yr, age >75yr), both male and female, by determining the trabecular thickness and spacing in the longitudinal and transverse directions (trabecular strut thickness is typically 0.1mm and spacing between struts in the order of 1mm, although as stated above this varies substantially with the degree of osteoporosis). The trabecular lattice FE model was comprised of longitudinal and transverse beams of thickness and spacing as reported by Mosekilde[28]. The single trabeculae model previously described was used to represent the load bearing longitudinal struts, and the transverse struts which provide the ties between the longitudinal struts were represented using two node linear beam elements.

Lattice perturbation

Each vertex point in the (initially) regular lattice was perturbed to provide a degree of irregularity as is observed in real bone. Based on a previous study by Silva & Gibson[25]

a perturbation factor of 0.3 was used, hence each vertex node was randomly moved by a distance in the range ±0-30% of the trabecular spacing value in any direction. The actual distance moved was randomly generated according to a Gaussian (normal) distribution. A qualitative comparison between the resulting trabecular bone lattice and real aged human trabecular bone is shown in Figure 2.

Cylindrical core geometry

The overall geometry of the trabecular bone lattice models (bone cylinders of height 10 mm and radius 3.5 mm) was defined to match the dimensions of cylindrical trabecular bone core biopsy specimens tested by Mosekilde[28], to allow comparison of the predicted and experimentally measured trabecular core stiffness and strength. In the lattice models, intersecting struts shared a common node at their junction, so that all degrees of freedom at these intersection nodes were equal for the strut ends connected to them.

Mesh density

As previously mentioned, each longitudinal trabecular strut was modelled using two quadratic beam elements. The age <50yr trabecular core model consisted of approximately 3,000 elements, and the age >75yr trabecular core consisted of approximately 500 elements.

Material properties

Trabecular bone tissue level material properties were applied based on reported values for human trabecular bone tissue[22,29,30]. Two material definitions were applied to each model to investigate the importance of plasticity in the models. The first was an isotropic linear elastic material definition (E=8GPa, ν= 0.3) and the second included a

von Mises yield criteria with perfect plasticity post-yield (E=8GPa, ν= 0.3, σ_y = 64 MPa).

Loads and boundary conditions

The boundary and loading conditions aimed to replicate the experimental conditions. All the nodes on the upper and lower end faces of the cylinder were constrained in the transverse degrees of freedom (to represent the enclosing end-caps which are used in experimental compression tests of trabecular bone core biopsy specimens). Nodes on the upper end face were displaced by -2 mm in the axial direction while nodes on the lower face were constrained in this direction. Figure 3 shows the resulting cylindrical trabecular core model with constrained nodes simulating the end-caps shown in red.

Solution type

Quasi-static large displacement solutions were performed using ABAQUS/Standard (Simulia, RI, USA). The models were solved with the ABAQUS 'stabilise' function enabled. The 'stabilise' function provided damping for local instabilities in the unstable systems, allowing the solution to be tracked for beams undergoing buckling failure.

Analysis of results

The apparent mechanical properties of the trabecular core models were determined and compared to apparent properties determined experimentally from *in vitro* mechanical tests on human trabecular core specimens by previous authors. The apparent compressive strength of each model was calculated as the apparent axial stress (total vertical reaction force divided by nominal cylindrical core cross-sectional area) reached in the simulation at trabecular core failure (defined as the point at which the force vs

displacement curve for the model reached approximately zero gradient), and was compared with the experimentally determined apparent compressive strength of the corresponding experimentally tested trabecular core specimens[28]. The apparent Young's modulus was determined using the linear region of the predicted FE model apparent stress/strain response, between 0 and 0.4% apparent compressive strain. The ultimate apparent strain was the strain at the point of failure (as defined above). As Mosekilde[28] did not report the apparent Young's modulus or ultimate strain of these specimens, the model predictions for apparent elastic modulus and ultimate strain were compared against another set of experimental data, reported by Kopperdahl and Keaveny[31] for human vertebral trabecular bone core specimens (age range 32 – 65 years) that also underwent axial compression testing.

Whole vertebral body model

Model geometry and trabecular structure

Finally, the trabecular bone microstructural model was enclosed by a thin layer of shell elements, representing the vertebral cortex. The three female trabecular micro-structures derived from Mosekilde[28] (age < 50yr, age 50-75yr and age > 75yr) were further developed to produce vertebral body models of three representative age ranges (Figure 4). The vertebral body geometry was based on parametric equations described by Mizrahi which describe the 'average' anatomy of an L3 lumbar vertebral body. Varying the parameters in Mizrahi's equation allows systematic variation of the vertebral body geometry[16]. The equations imply both a sagittal and transverse symmetry plane, which was utilised to reduce the model size and develop quarter vertebral body models. The posterior elements of the vertebra were not included in the

model as they have been found to play a minor role during compressive loading of the anterior vertebral body[32].

The vertebral body was created by warping a hollow cylinder, meshed using four node, reduced integration, linear shell elements (S4R element type in ABAQUS), to fit the Mizrahi equations[16]. The vertebral cortex is a thin layer of dense cortical bone, and accordingly the shell element thickness was specified as 0.5 mm, based on reported measured thickness values[33]. With aging and the progression of osteoporosis, the vertebral cortex thins further, and therefore the age > 75 models were also produced with a wall thickness of 0.2 mm, based on reported measured thickness values of aged vertebrae[33]. A mesh sensitivity analysis was performed to determine an appropriate in-plane element size for the cortical shell mesh.

Tie and symmetry constraints

The ABAQUS tie constraint function was used to connect the trabecular beam elements at the cortical shell interface to the shell elements. The tie constraints between the trabecular beams and the outer shell tie all degrees of freedom together, so that the beam ends are fixed to the shell for both translational and rotational degrees of freedom. As the model included both transverse and sagittal symmetry planes, ABAQUS symmetry plane boundary conditions were applied to all nodes on the section plane. The symmetry plane boundary conditions prevent translation through the symmetry plane, and only allow rotation around the axis perpendicular to the symmetry plane.

Material properties

The tissue material properties were assumed to be the same for trabecular bone and cortical bone, as is commonly assumed in FE modelling as the mechanical properties for the two bone types are highly similar at the tissue level[30,34-36]. An elastic, perfectly plastic von Mises material definition was applied, as previously described.

Load cases

Two different loading cases were applied to the whole vertebral body models, to simulate (i) common *in vitro* experimental loading conditions used for testing the compressive strength of cadaveric human lumbar vertebrae, and (ii) relaxed standing, a physiologically realistic load case.

For *in vitro* testing of cadaveric vertebral specimens, an isolated vertebral body is commonly mounted between two rigid platens using polymer bone cement, and the specimen is then compressed to failure in a uniaxial testing machine, with one of the platens mounted on a ball joint to avoid introducing moments during the test. To simulate this loading case, all nodes on the upper endplate were attached to an ABAQUS multi-point constraint (MPC) node, which was held in the transverse planes, and displaced -6mm in the axial (*z*) plane. Full rotation was allowed at the MPC node, to simulate the ball joint used during *in vitro* compressive strength testing of cadaveric vertebral body specimens.

To simulate the physiological load case of relaxed standing, a uniform pressure load of 0.3MPa was applied to the entire upper endplate of the vertebra model. Based on previous intradiscal pressure measurement studies[38,39], nucleus pulposus pressure in the intervertebral disc during relaxed standing is around 0.5 MPa, and as the nucleus pressure is 1.5 times the average pressure over the endplate[38], a uniform pressure of 0.3 MPa was applied over the entire vertebral endplate to approximate standing.

Analysis of results

The predicted vertebral stiffness was determined from the linear region (0 to 0.1 mm displacement) of the force displacement curve for the *in-vitro* load case models, and the predicted strength was the peak force reached during the simulation (shown schematically in Figure 5). Both predicted stiffness and strength were compared to reported experimentally determined values. The tissue level strains within each trabeculae were analysed, and the maximum strains (either tensile or compressive) at the beam element integration points were determined and displayed graphically using histograms.

Results

Single trabeculae model

Figure 6 shows a plot of the FE predicted failure force for the elastic-perfectly plastic stainless steel column models versus the experimentally measured failure force for the columns. The single strut model predicted the critical forces associated with both elastic buckling and plastic collapse failure mechanisms across a wide range of slenderness ratios with a mean error of 8% and a maximum error of 19%.

Trabecular bone lattice model

The predicted apparent compressive stress of the various trabecular bone models are compared against the corresponding experimentally measured values in Figure 7[28]. The predicted apparent Young's modulus and ultimate strain of the models are compared against the experimentally measured values from Kopperdahl & Keaveny in Table 1[31].

Figure 7 shows that a purely elastic material model considerably overestimated the apparent stress for all models. However, the use of the elastic perfectly plastic model demonstrated apparent compressive properties which were within one standard deviation of the experimental data for all models.

Vertebral body model

The predicted vertebral body stiffness and maximum compressive strength for the vertebral body models subjected to simulated *in vitro* loading are given in Table 2. Figure 8 shows contours of maximum (most tensile) and minimum (most compressive) principal strain in the vertebral cortical shell and trabecular core tissue for the age > 75 model. The contour plots in Figure 8 were generated at the point when an apparent (compressive) strain of -0.5% had been applied to the vertebral body. By comparison, the tissue level uniaxial yield strain for the material properties used in the simulations was 0.8%. For the simulated physiological (relaxed standing) load case, Figure 9 compares the deformed shape of the age < 50 and age > 75 vertebral models under the 0.3MPa applied pressure load, and the deformed shape at failure is also shown for both models for comparison. Histograms of predicted tissue strain within the trabecular core under the simulated *in vivo* load case are shown in Figure 10.

Discussion

Osteoporotic vertebral compression fractures occur primarily due to reduced bone density and changes in the vertebral trabecular micro-structure. In particular, the change in slenderness ratio of longitudinal trabecular struts means that it is important to capture the micro-mechanics of trabecular bone failure in order to correctly predict the overall vertebral response to load with progressive osteoporosis. Modelling studies to

date have either focussed on the whole vertebral body, assuming highly simplified continuum behaviour for the trabecular core, or modelled small regions of the trabecular core in isolation. The multi-scale nature of the problem has hindered investigation into the internal trabecular mechanics and apparent vertebral mechanics simultaneously. This work has presented the development of a multi-scale FE model of a human L3 lumbar vertebral body with an internal trabecular micro-structure, which can be used to explore the coupling between changes in trabecular bone micro-mechanics with osteoporotic bone loss, and overall compressive response of the whole vertebral body.

A parametric vertebral body FE model was developed based on equations by Mizrahi[16], which is a geometrically idealised representation of a real human vertebra. While this geometry does not replicate an actual vertebral body, this approach enables systematic variation of vertebral body geometry, and provides a generalized representation of lumbar vertebra anatomy based on a large population. The vertebral body model did not include the posterior elements or adjoining soft tissue. As vertebral compression fractures occur due to the collapse of the anterior vertebral body in isolation, other structures were excluded to avoid unwarranted computational expense and model complexity. Although the posterior elements are not of great importance in compressive loading, future work could include simulation of the intervertebral discs adjacent to the vertebral body endplates to allow more physiological loading conditions to be applied. Additionally, contact between the individual beam elements of the trabecular micro-structure was not modelled, and hence any effect of densification occurring due to contact between trabeculae was not incorporated in the model predictions. Due to the small strains applied, and the small local displacements of the

elements, it is unlikely that adjacent trabecular struts would contact until well after the initiation of failure of the vertebral body.

In developing the multi-scale FE models, a single longitudinal trabecular strut model was developed first, to ensure that the basic strut model was able to correctly produce buckling behaviour for a range of buckling regimes. The trabecular strut model used (two quadratic finite elements with full integration) was able to capture the range of failure mechanisms of a column, from plastic collapse to purely elastic buckling, with a mean error of 8% compared to experimental data[28]. While more elements could have been used for increased accuracy, computational efficiency of the trabecular mesh was vital due to the large number of trabeculae required in the full vertebral body model. The simple configuration of two quadratic elements proved an efficient model for a single trabeculae strut while keeping errors in predicted buckling force below 10%. In the previously mentioned preliminary analysis used to determine the initial beam offset, we assessed the effect of initial imperfection offset on predicted buckling response, and found that initial imperfections between 0.001 and 0.01mm (for a 1.1mm quadratic beam element of radius 0.1mm) gave buckling forces between 6.7% and 7.5% higher than the analytical (Euler) solution respectively. So there is a small effect of initial imperfection on predicted buckling force in this range, which may be partially responsible for the change in the FE results curve in Figure 6 at a slenderness ratio of around 50.

The importance of incorporating bone tissue yielding was highlighted in the elastic, and elastic-perfectly plastic, trabecular bone models. When comparing FE solutions with experimental data on trabecular bone cores from Mosekilde[28], the elastic trabecular

models were able to predict the maximum axial stress within one standard deviation for the age > 75 models, however there was increasing error with reduced age. With the inclusion of a von Mises yield criteria and perfect plasticity post-yield in the bone tissue material description, all model predictions were within one standard deviation of the experimental results. This result suggests that healthy bone fails mainly due to yielding of the material, and hence plasticity is required for an accurate model. However, as bone ages it becomes more susceptible to elastic buckling, which was captured in the purely elastic age >75yr models.

With the inclusion of plasticity, the trabecular bone models were able to predict the maximum compressive strength of the corresponding experimentally tested trabecular specimens to within one standard deviation of the experimental results. The predicted Young's modulus and maximum compressive strength of the age < 50yr and age 50-75yr specimens were also within the range predicted by Kopperdahl and Keaveny, though the age > 75yr models were slightly below the reported range[31]. As Kopperdahl and Keaveny used trabecular specimens from an age range of 32 to 65 years, the underestimation of the age > 75yr models is to be expected[31]. The predicted ultimate strain of the trabecular models was in the experimental range reported by Kopperdahl and Keaveny for all age groups[31]. These results provide confidence that the modelling approach used (i.e. a perturbed lattice of beam elements, with an elastic perfectly plastic von Mises material definition) is capable of predicting trabecular bone apparent properties in reasonably good agreement with experimental measurements on cadaveric human trabecular bone specimens.

In vitro experimental investigations of human cadaveric vertebral bodies have shown vertebral compressive strength decreases from around 60MPa at age 20 to around 2.6MPa at age 80[37]. Due to variations in specimen age, loading conditions, and trabecular density, it is difficult to directly compare the whole vertebral body predictions with experimentally reported results. Even so, the predicted compressive strength in the vertebral body models with a wall thickness of 0.5 mm ranged from 4.5 MPa in the age <50yr case, to 2.6 MPa in the age >75yr case. Further thinning the cortical shell to 0.2mm (which would represent severe osteoporosis in a very elderly patient) reduced the predicted compressive strength to 1.0MPa (Table 2). The relative decrease in predicted vertebral strength obtained with the multi-scale FE models again provides confidence in the models' ability to realistically represent the mechanics of human vertebrae.

The histograms of Figure 10 show that local tissue strains within the trabeculae become less uniform, and increase in magnitude, with the progression of age and osteoporosis. While the age <50yr and age 50-75yr models predict no tissue level strains beyond the tissue level yield point, the age >75yr model does have a number of trabeculae beyond the yield limit, indicating these trabeculae would have failed even under the relatively mild physiological loading case of relaxed standing. This demonstrates the ability of multi-scale modelling approaches to predict tissue level strains and failure mechanisms within the trabecular micro-structure for physiologically meaningful compressive loading conditions applied to the entire vertebral body. We note that there is a limitation on the prediction of tissue level strain using the current modelling approach, in that the beam elements are assumed to have constant cross-section, whereas it is known that actual trabeculae taper, reducing in thickness toward the centre of the strut. The beam

elements will therefore tend to underpredict trabecular tissue strains at the centres of the struts, and overpredict strain at the strut junctions. However, this is not a fundamental limitation of the model, as varying cross-section struts could be simulated using tapered beam elements in a future study, if quantitative dimensions for the varying strut cross-section in osteoporotic trabecular bone were available.

In summary, this work has presented the development of a novel, multi-scale Finite Element model of an osteoporotic vertebral body which provides a potentially useful tool for investigating the mechanisms of vertebral compression fractures both at the trabecular micro-structural level, and at the whole vertebral body level. This model can be used in future studies to explore the mechanical relationship between the trabecular core and vertebral body, allowing detailed prediction of the mechanisms of vertebral compression fracture which occur in osteoporosis.

References

1. Anon. Consensus development conference: Diagnosis, prophylaxis and treatment of osteoporosis. in American Journal of Medicine. 1993;94:646-50.
2. Lin JT, Lane, J.M. Osteoporosis: A review. Clin Orthop Relat Res. 2004; 425: 126-34.
3. Riggs BL and Melton LJ, 3rd. The worldwide problem of osteoporosis: Insights afforded by epidemiology. Bone. 1995; 17(5): 505S-511S.
4. Borah B, Gross, G.J., Dufresne, T.E., Smith, T.S., Cockman, M.D., Chmielewski, P.A., Lundy, M.W., Hartke, J.R., Sod, E.W. Three-dimensional microimaging, finite element modelling, and rapid prototyping provide unique insights into bone architecture in osteoporosis. Anatomical Record. 2001; 265(2): 101-110.
5. Nevitt MC, Ross PD, Palermo L, Musliner T, Genant HK, and Thompson DE. Association of prevalent vertebral fractures, bone density, and alendronate treatment with incident vertebral fractures: Effect of number and spinal location of fractures. The fracture intervention trial research group. Bone. 1999; 25(5): 613-619.
6. Johnell O, Kanis JA, Oden A, Sernbo I, Redlund-Johnell I, Petterson C, De Laet C, Jönsson B. Mortality after osteoporotic fractures. Osteoporosis International. 2004;15:38-42.
7. Singer K, Edmondston S, Day R, Breidahl P, and Price R. Prediction of thoracic and lumbar vertebral body compressive strength: Correlations with bone mineral density and vertebral region. Bone. 1995; 17(2): 167-174.
8. Bono CM and Einhorn TA. Overview of osteoporosis: Pathophysiology and determinants of bone strength. European Spine Journal. 2003; 12(Supplement 2): S90-S96.
9. Rockoff SD, Sweet E, and Bleustein J. The relative contribution of trabecular and cortical bone to the strength of human lumbar vertebrae. Calcified Tissue Research. 1969; 3(2): 163-175.
10. Andresen R, Werner HJ, and Schober HC. Contribution of the cortical shell of vertebrae to mechanical behaviour of the lumbar vertebrae with implications for predicting fracture risk. British Journal Of Radiology. 1998; 71(847): 759-765.
11. Hildebrand T. Direct three-dimensional morphometric analysis of human cancellous bone: Microstructural data from spine, femur, iliac crest, and calcaneus. Journal Of Bone And Mineral Research. 1999; 14: 1167-1174.
12. Mosekilde L. Vertebral structure and strength in vivo and in vitro. Calcified Tissue International. 1993; 53(Supplement 1): S121-S125.
13. Bell GH, Dunbar O, Beck JS, and Gibb A. Variations in strength of vertebrae with age and their relation to osteoporosis. Calcified Tissue International. 1967; 1(1): 75-86.
14. Adams MF, Bayraktar HH, Keaveny TM, and Papadopoulos P. Ultrascalable implicit finite element analyses in solid mechanics with over a half a billion degrees of freedom. in ACM/IEEE Proceedings of SC2004: High Performance Networking and Computing 2004.
15. Polikeit A, Nolte LP, and Ferguson SJ. Simulated influence of osteoporosis and disc degeneration on the load transfer in a lumbar functional spinal unit. Journal of Biomechanics. 2004; 37(7): 1061-1069.

16. Mizrahi J, Silva, M.J., Keaveny, T.M., Edwards, W.T., Hayes, W.C. Finite-element stress analysis of the normal and osteoporotic lumbar vertebral body. Spine. 1993; 18(14): 2088-2096.
17. Wilcox R, Allen DJ, Hall RM, Limb D, Barton DC, and Dickson RA. A dynamic investigation of the burst fracture process using a combined experimental and finite element approach. European Spine Journal. 2004; 13(6): 481-488.
18. Wijayathunga VN, Jones AC, Oakland RJ, Furtado NR, Hall RM, and Wilcox RK. Development of specimen-specific finite element models of human vertebrae for the analysis of vertebroplasty. Proceedings of the Institution of Mechanical Engineers; Journal of Engineering in Medicine; Part H; London. 2008; 222: 221-8.
19. Wilcox RK. The influence of material properties and morphological parameters on specimen-specific finite element models of porcine vertebral bodies. Journal of Biomechanics. 2007; 40: 669-673.
20. Bayraktar HH and Keaveny TM. Mechanisms of uniformity of yield strains for trabecular bone. Journal of Biomechanics. 2004; 37(11): 1671-1678.
21. Bevill G, Eswaran SK, Gupta A, Papadopoulos P, and Keaveny TM. Influence of bone volume fraction and architecture on computed large-deformation failure mechanisms in human trabecular bone. Bone. 2006; 39(6): 1218-1225.
22. Niebur GL, Feldstein MJ, Yuen JC, Chen TJ, and Keaveny TM. High-resolution finite element models with tissue strength asymmetry accurately predict failure of trabecular bone. Journal of Biomechanics. 2000; 33(12): 1575-1583.
23. Chevalier Y, Pahr D, Allmer H, Charlebois M, and Zysset P. Validation of a voxel-based FE method for prediction of the uniaxial apparent modulus of human trabecular bone using macroscopic mechanical tests and nanoindentation. Journal of Biomechanics. 2007; 40(15): 3333-3340.
24. Pothuaud L, Van Rietbergen B, Charlot C, Ozhinsky E, and Majumdar S. A new computational efficient approach for trabecular bone analysis using beam models generated with skeletonized graph technique. Computer Methods in Biomechanics And Biomedical Engineering. 2004; 7(4): 205-213.
25. Silva MJ, Gibson, LJ. Modeling the mechanical behavior of vertebral trabecular bone: Effects of age-related changes in microstructure. Bone. 1997; 21(2): 191-199.
26. Vajjhala S, Kraynik AM, and Gibson LJ. A cellular solid model for modulus reduction due to resorption of trabeculae in bone. Journal of Biomechanical Engineering. 2000; 122(5): 511-515.
27. Rahman MA, Tani J, and Afsar AM. Postbuckling behaviour of stainless steel (sus304) columns under loading-unloading cycles. Journal of Constructional Steel Research. 2006; 62(8): 812-819.
28. Mosekilde L. Sex differences in age-related loss of vertebral trabecular bone mass and structure--biomechanical consequences. Bone. 1989; 10(6): 425-432.
29. Rho J-Y, Kuhn-Spearing L, and Zioupos P. Mechanical properties and the hierarchical structure of bone. Medical Engineering & Physics. 1998; 20(2): 92-102.
30. Bayraktar HH, Morgan EF, Niebur GL, Morris GE, Wong EK, and Keaveny TM. Comparison of the elastic and yield properties of human femoral trabecular and cortical bone tissue. Journal of Biomechanics. 2004; 37(1): 27-35.
31. Kopperdahl D and Keaveny T. Yield strain behavior of trabecular bone. Journal of Biomechanics. 1998; 31(7): 601-608.

32. Hongo M, Abe, E., Shimada, Y., Murai, H., Ishikawa, N., Sato, K. Surface strain distribution on thoracic and lumbar vertebrae under axial compression. The role in burst fractures. Spine. 1999; 24(12): 1197-1202.
33. Mosekilde L. Vertebral structure and strength in vivo and in vitro. Calcified Tissue International. 1993; 53(Supplement 1): S121-S125; discussion S125-S126.
34. Turner CH, Rho J, Takano Y, Tsui TY, and Pharr GM. The elastic properties of trabecular and cortical bone tissues are similar: Results from two microscopic measurement techniques. Journal of Biomechanics. 1999; 32(4): 437-441.
35. Keaveny TM, Guo XE, Wachtel EF, McMahon TA, and Hayes WC. Trabecular bone exhibits fully linear elastic behaviour and yields at low strains. Journal of Biomechanics. 1994; 27(9): 1127-1129.
36. Rho JY, Tsui TY, and Pharr GM. Elastic properties of human cortical and trabecular lamellar bone measured by nanoindentation. Biomaterials. 1997; 18(20): 1325-1330.
37. Mosekilde L and Leif M. Normal vertebral body size and compressive strength: Relations to age and to vertebral and iliac trabecular bone compressive strength. Bone. 1986; 7: 207-212.
38. Nachemson A, Morris, J.M. In vivo measurements of intradiscal pressure. J Bone Joint Surg. 1964; 46: 1077-92.
39. Wilke HJ, Neef, P., Caimi, M., Hoogland, T., Claes, L.E. New in vivo measurements of pressures in the intervertebral disc in daily life. Spine. 1999; 24(8): 755-762.

Figure Captions

Figure 1. Sketch of two adjacent vertebrae showing the anterior vertebral body, posterior elements, internal trabecular bone core and thin cortical shell which surrounds the trabecular core. Note that the intervertebral disc between the two vertebral bodies is not shown.

Figure 2. Micro-CT image of aged vertebral trabecular bone (left). Magnified section view of trabecular bone model lattice (right) with 0.3 lattice perturbation factor,

Figure 3. Finite Element Model of cylindrical core of trabecular bone. The red nodes in the right hand figure show the constrained regions simulating the upper and lower end-caps which are used for in-vitro testing of trabecular bone specimens.

Figure 4. 3D vertebral body models for age <50yr (left), age 50-75yr (middle), and age >75yr (right), with 2D view of corresponding trabecular micro-structure.

Figure 5. Schematic compressive force versus displacement graph for vertebral body models showing maximum predicted vertebral strength in each case.

Figure 6. Comparison of FE predicted failure force for elastic-perfectly plastic beam models against experimental buckling forces for thin stainless steel columns with varying slenderness ratios (modelling the experiments of Rahman *et al.*[27]).

Figure 7. Comparison of experimental and FE (linear elastic and elastic-perfectly plastic) predicted maximum axial stress for trabecular bone models of various ages and genders. Experimental values are from Mosekilde[28].

Figure 8. Contours of (a) maximum principal strain in the cortical shell (b) minimum principal strain in the cortical shell, (c) maximum principal strain in the trabecular core, and (d) minimum principal strain in the trabecular core, for the age > 75yr vertebra model subjected to simulated *in vitro* loading. The contour plots were generated at the point when an apparent compressive strain of 0.5% had been applied to the vertebral body, to illustrate tissue strain distributions in the vertebra prior to apparent yield.

Figure 9. Deformed vertebral bodies under *in vivo* pressure loading showing the difference in predicted endplate deformation pattern between age < 50 and age >75 vertebra at a uniform endplate pressure of 0.3MPa, and at failure. Note that the deformations are scaled by factor of 10 for visualisation purposes.

Figure 10. Histograms of tissue level principal strains at a compressive endplate pressure load of 0.3MPa simulating relaxed standing (-x axis displays compressive principal and +x axis displays tensile principal strains) in trabeculae for (a) age <50yr, (b) age 50-75yr, (c) age >75yr vertebral body models. Dotted lines indicate the isotropic tissue level yield strain (0.8%).

Table 1. Predicted apparent elastic modulus, apparent strength, and apparent yield strain for the elastic-plastic trabecular bone lattice models, compared with the experimental data of Kopperdahl and Keaveny[31].

Trabecular core model		*E* (MPa)	Strength (MPa)	Ultimate strain (%)
Age <50yr	Female	253	2.84	2.12
	Male	267	2.96	2.39
Age 50-75yr	Female	138	1.21	1.71
	Male	183	1.72	1.80
Age >75yr	Female	74	0.54	1.05
	Male	61	0.60	1.60
Experimental (Kopperdahl and Keaveny[31], age range 32-65yrs)				
Mean ± SD		291 ± 113	2.23 ± 0.95	1.45 ± 0.33
Range		90-536	0.7-4.33	0.96-2.30

Table 2. Predicted stiffness and maximum compressive strength of vertebral bodies simulating various levels of osteoporosis (derived from simulated in-vitro loading models).

Model	Cortical shell thickness (mm)	Compressive stiffness (N/mm)	Max. compressive strength	
			(MPa)	(kN)
Age <50yr	0.5	26643	4.53	5.74
Age50-75yr	0.5	18736	3.21	4.06
Age >75yr	0.5	15274	2.59	3.28
Age >75yr	0.2	7983	0.99	1.25

Figure 1

Click here to download high resolution image

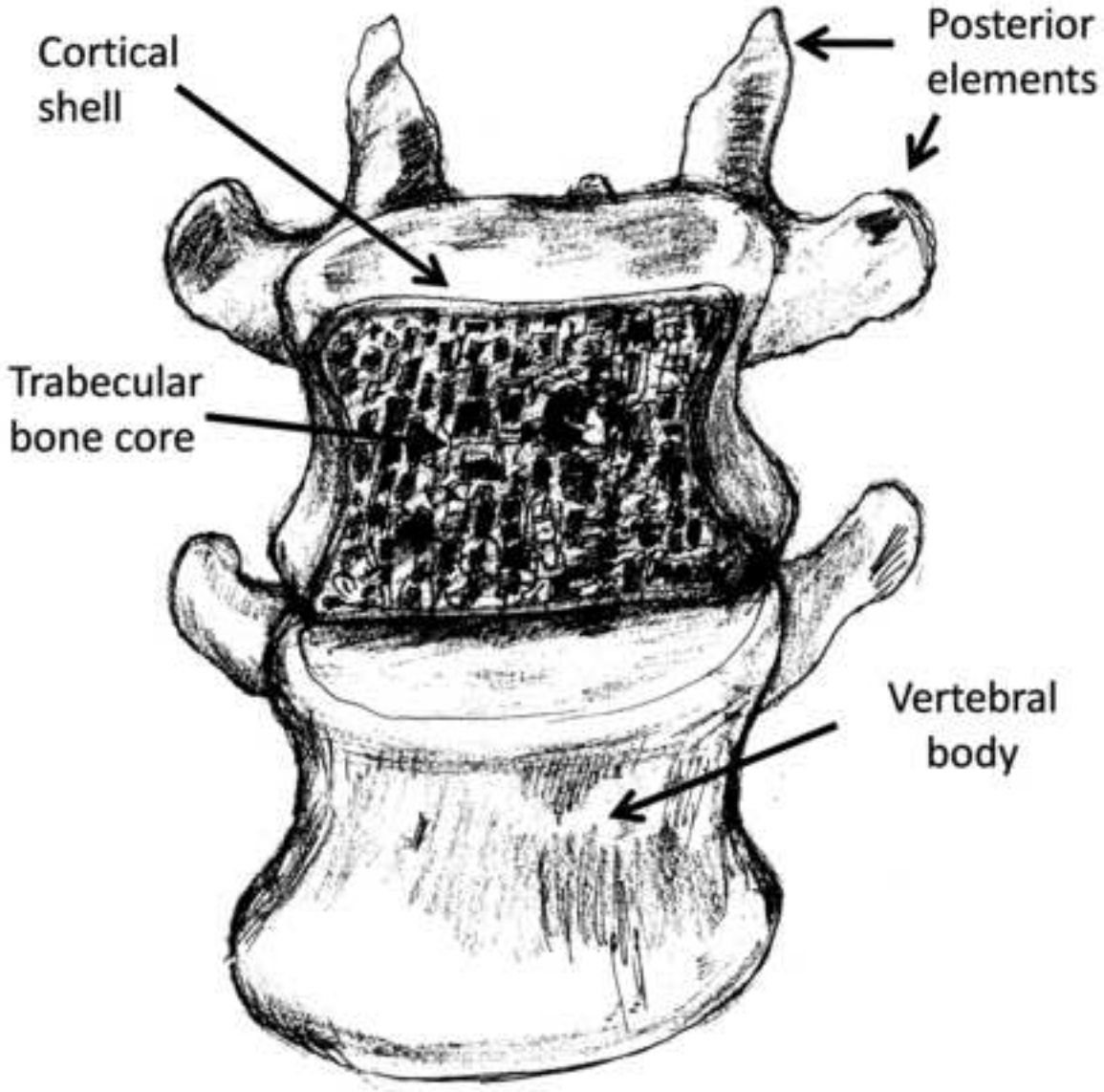

Figure 2

Click here to download high resolution image

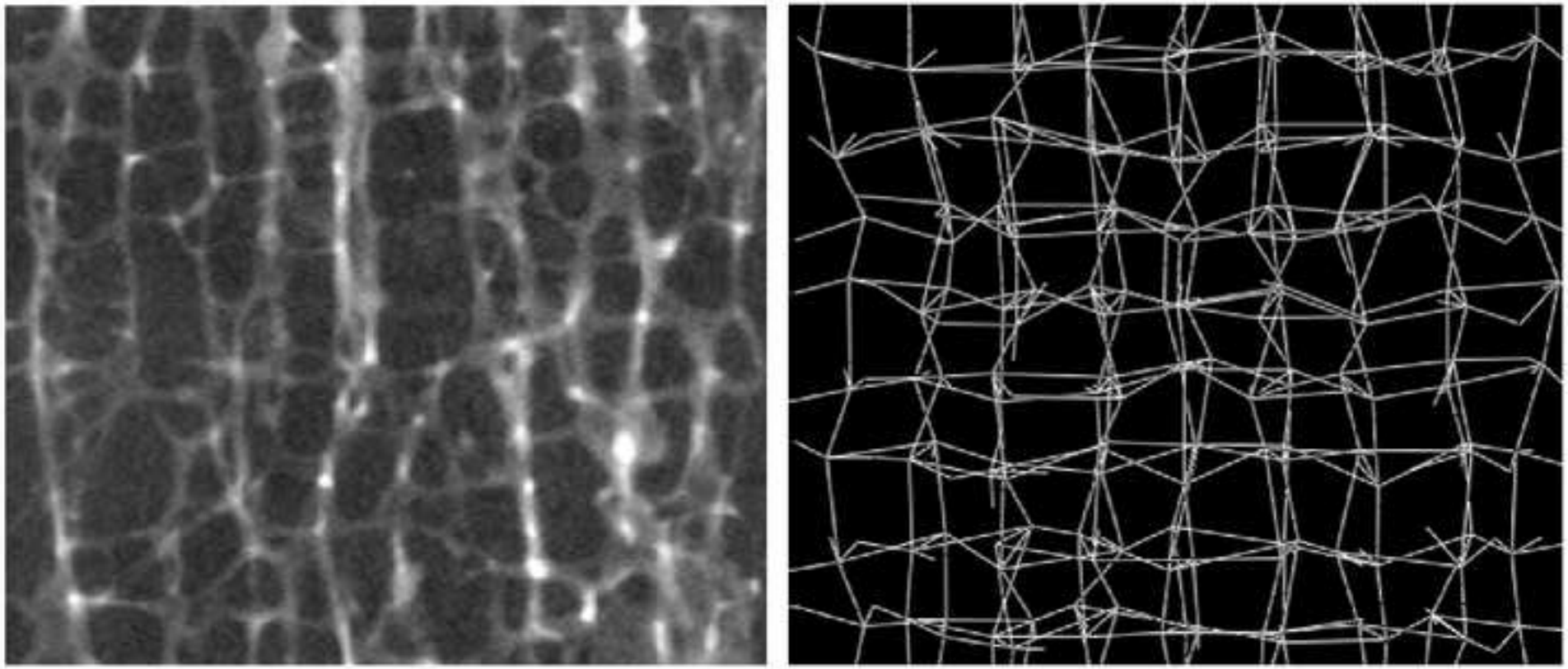

Figure 3

Click here to download high resolution image

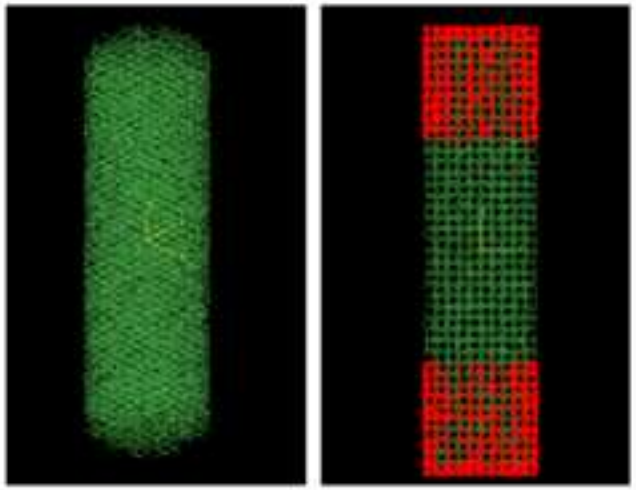

Figure 4

Click here to download high resolution image

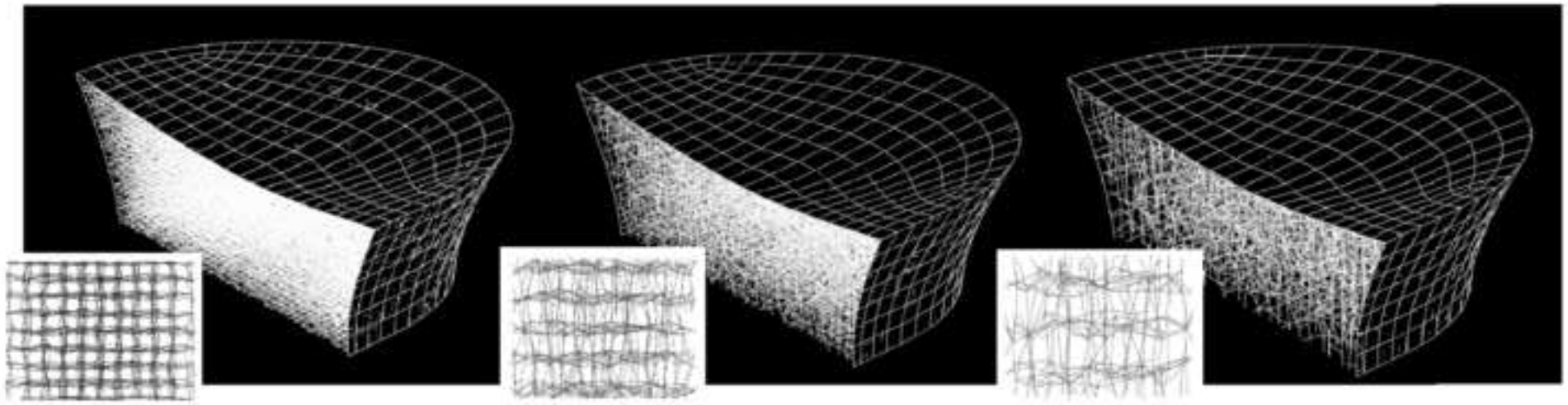

Figure 5

Click here to download high resolution image

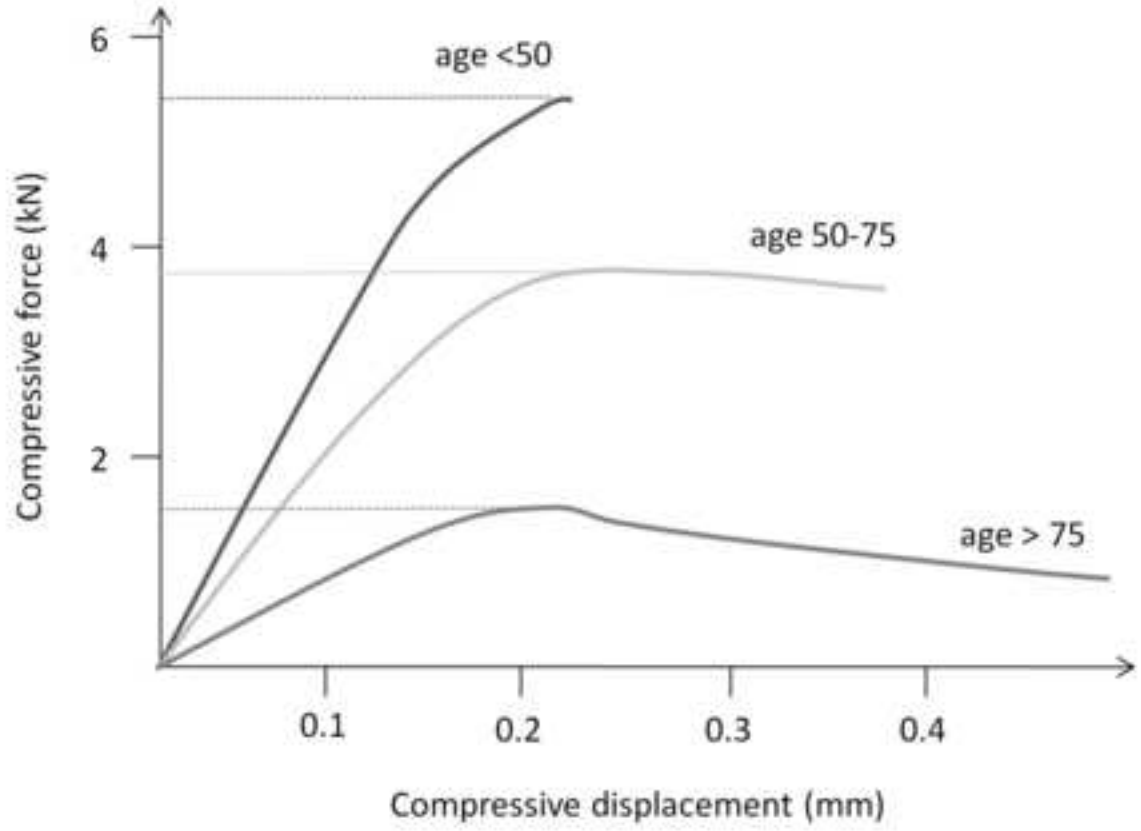

Figure 6
Click here to download high resolution image

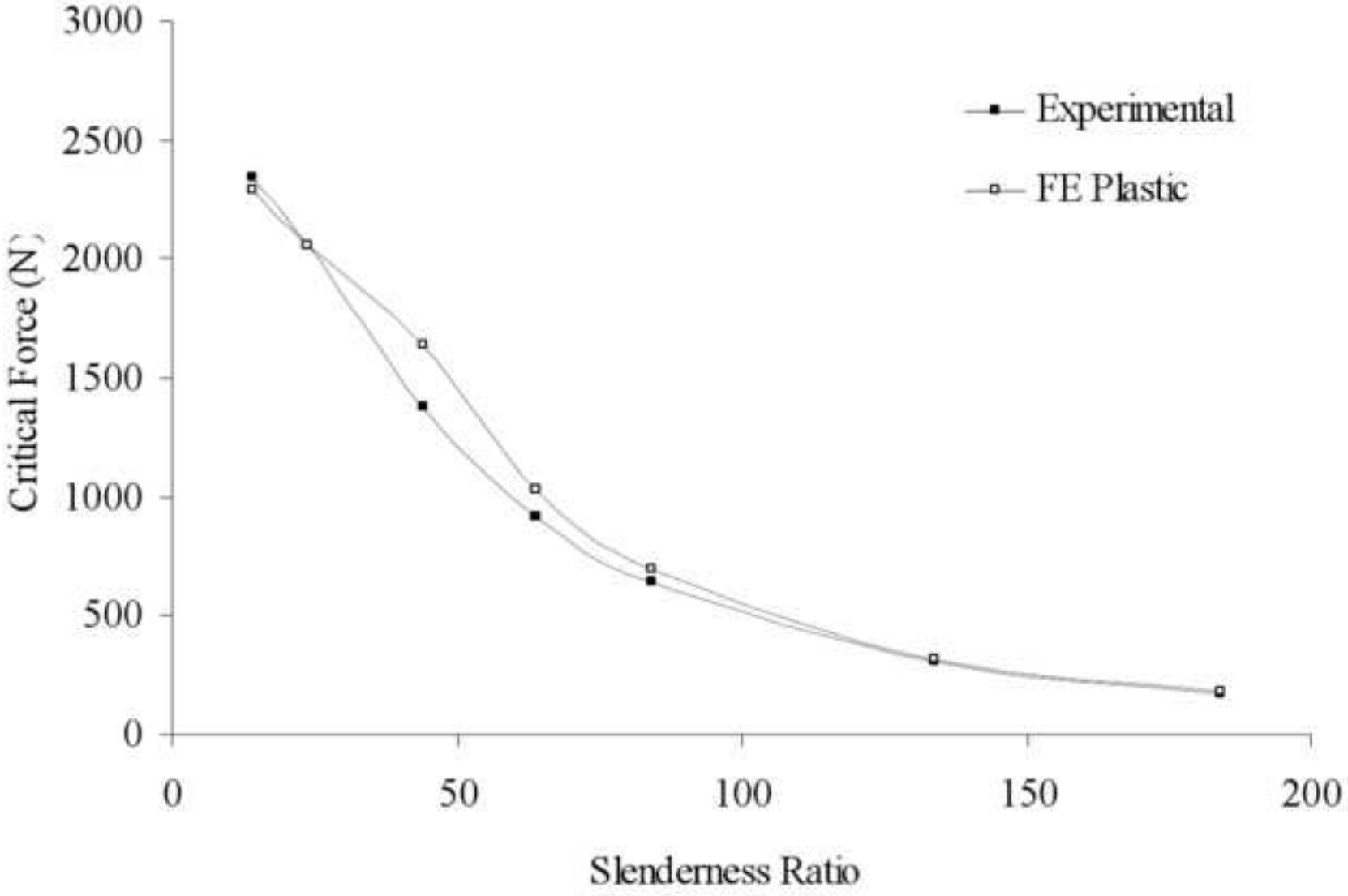

Figure 7

Click here to download high resolution image

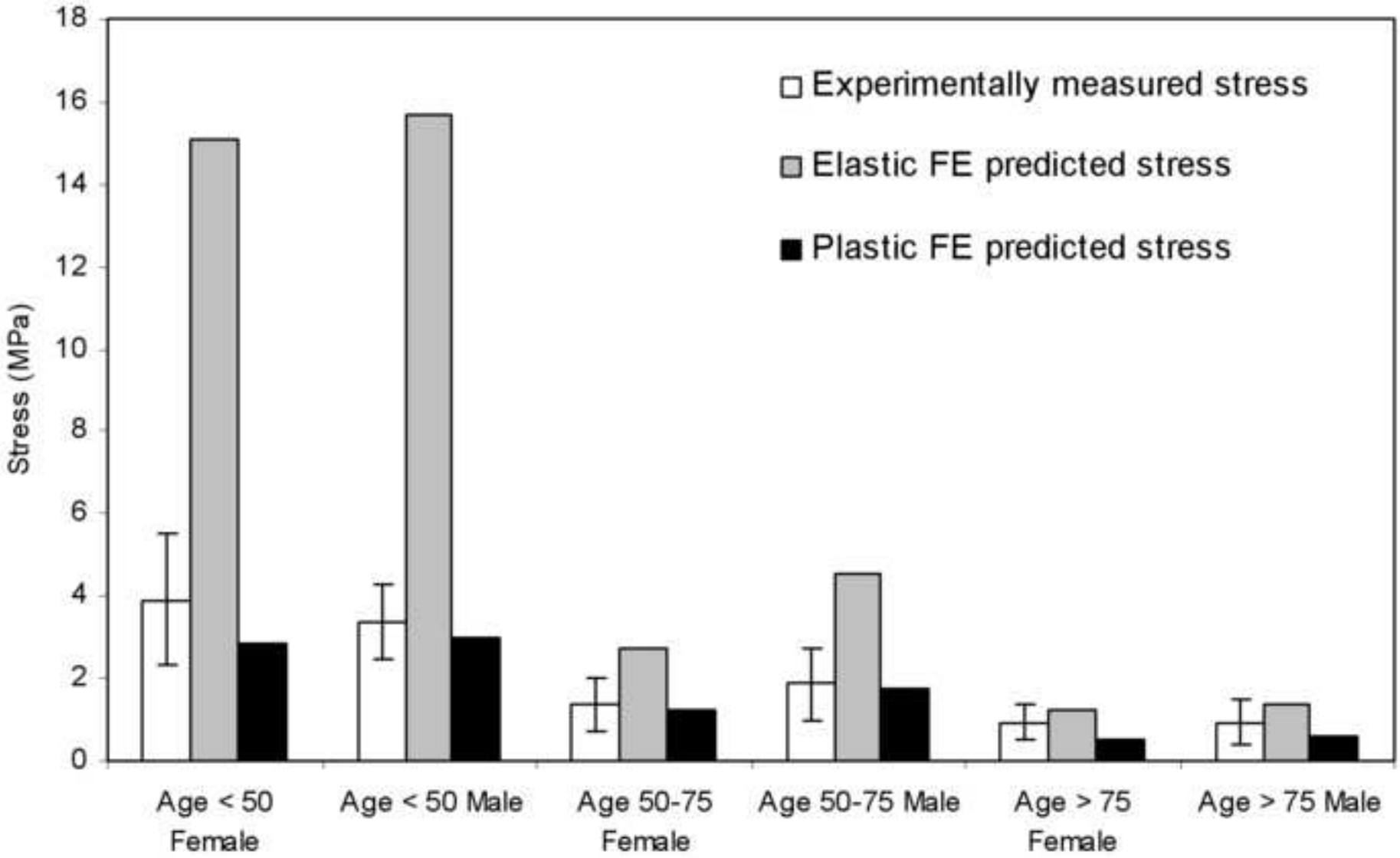

Figure 8

Click here to download high resolution image

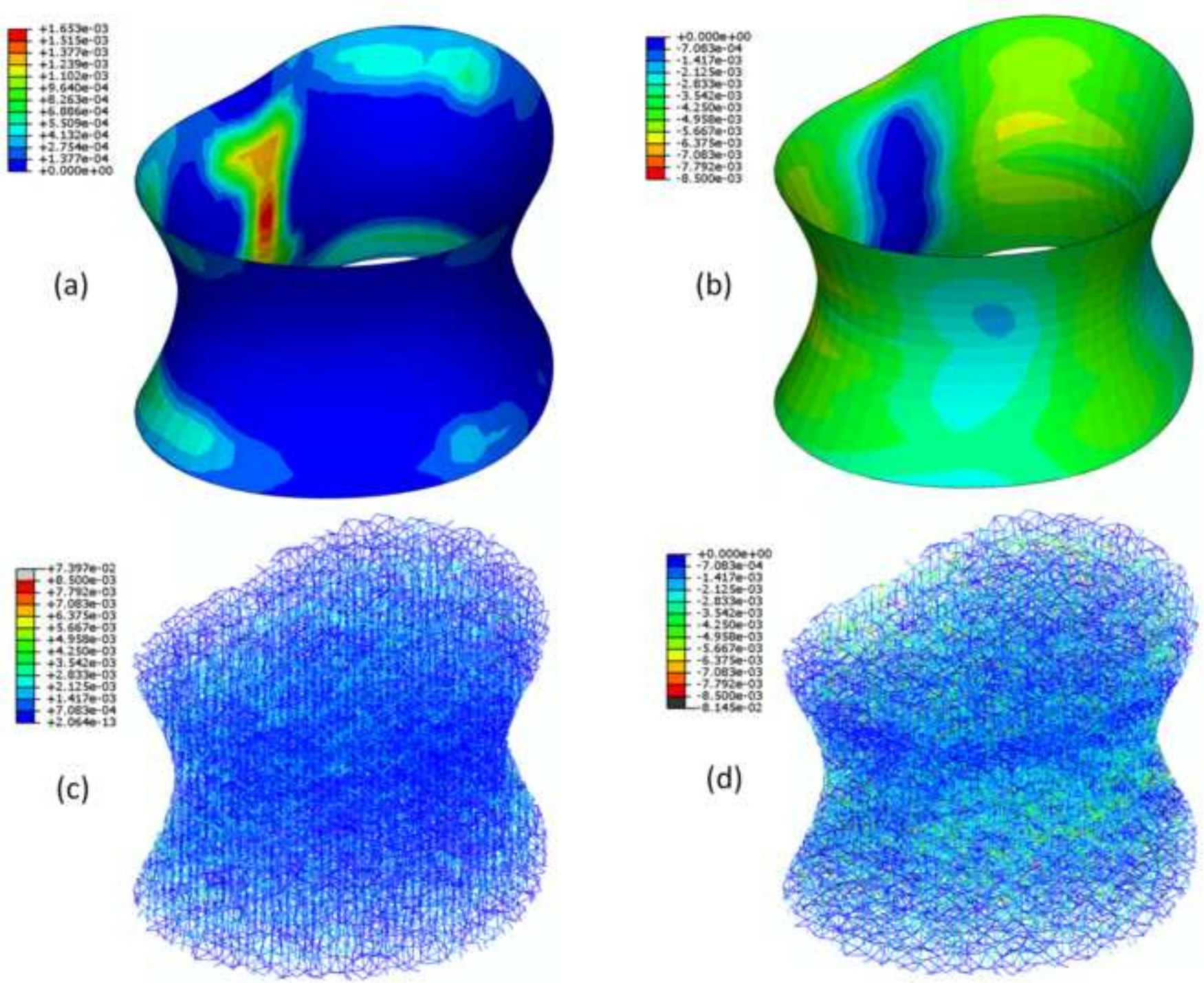

Figure 9

Click here to download high resolution image

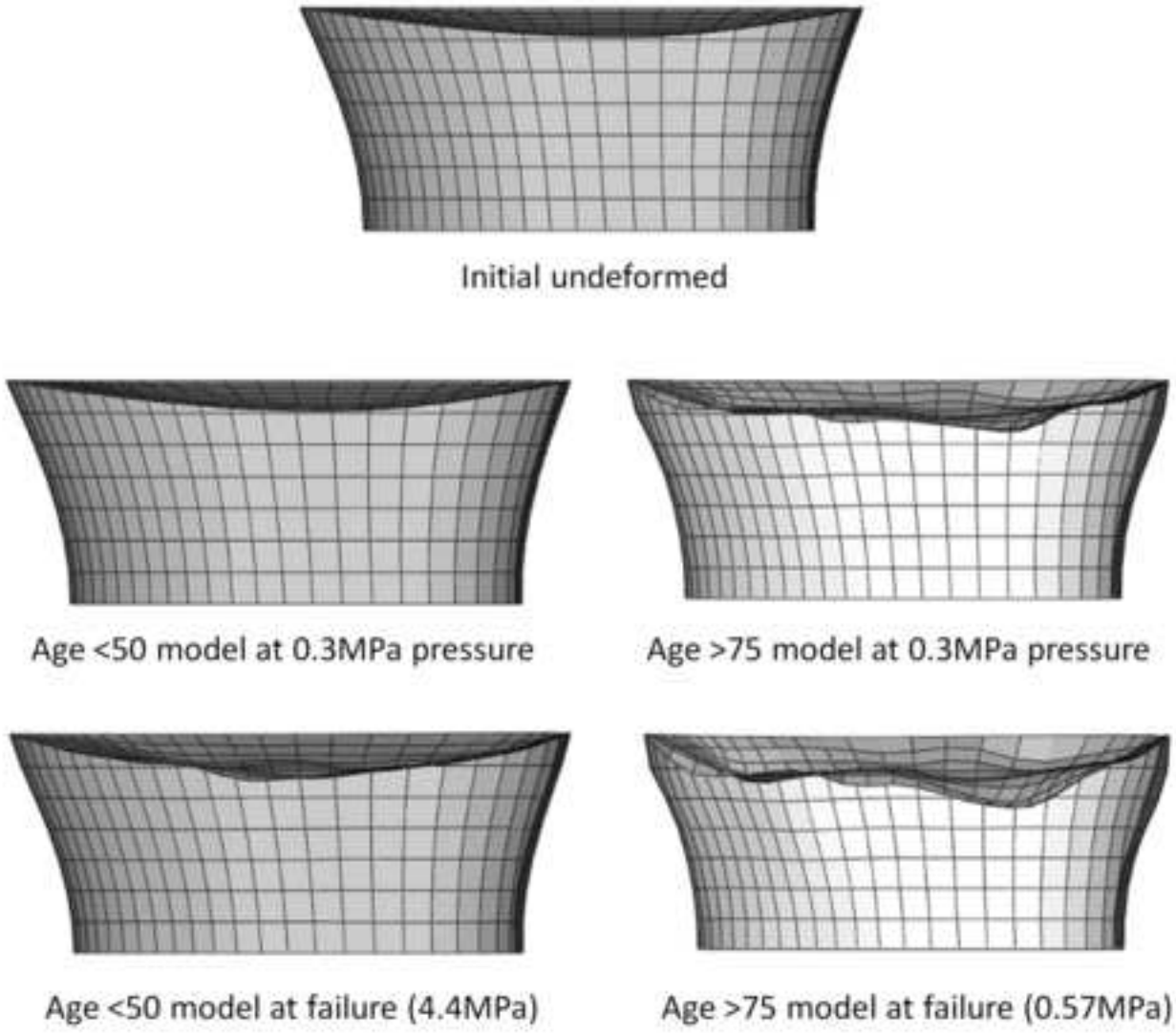

Figure 10

Click here to download high resolution image

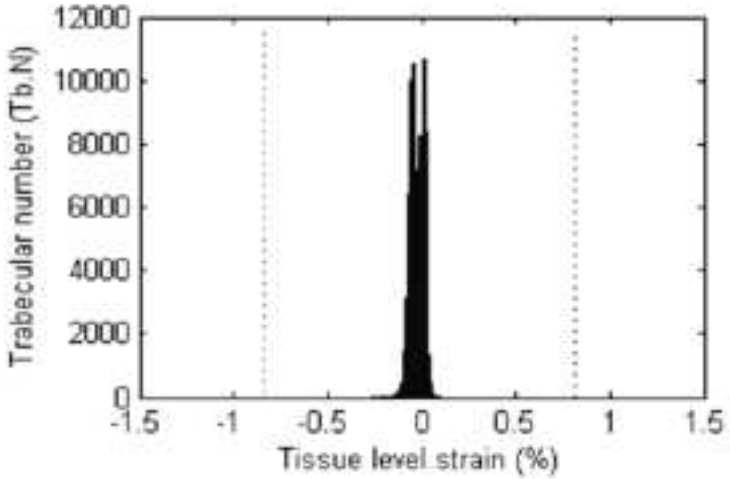

(a)

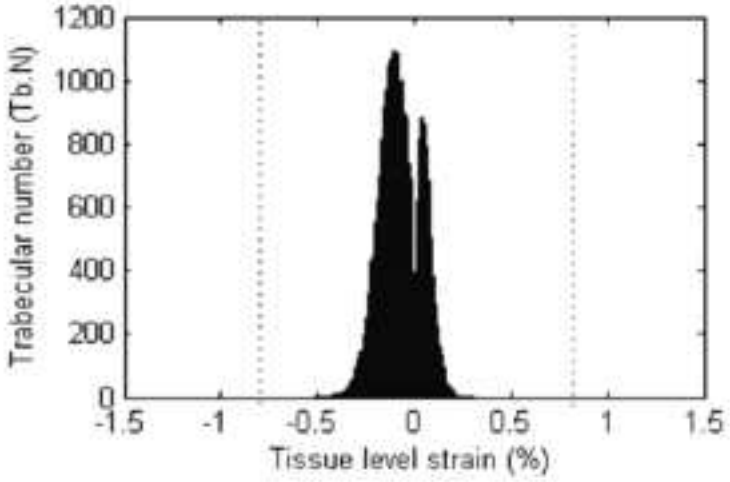

(b)

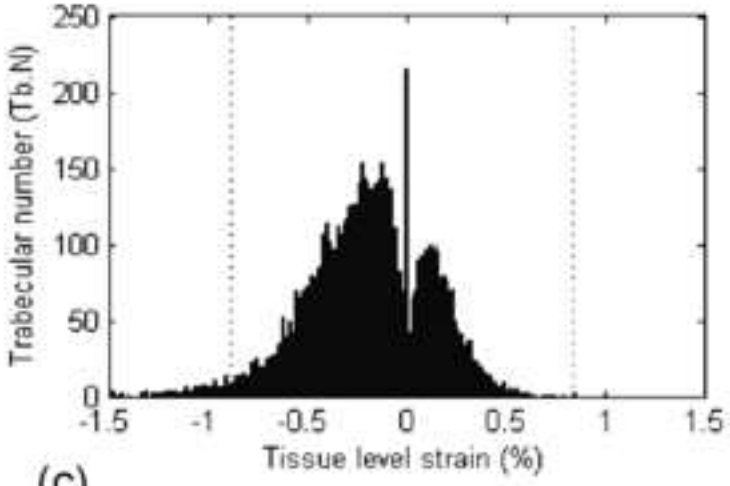

(c)